Advanced Nano Research
Volume 6, Issue 1, pp. 11-28, 2023
DOI: https://doi.org/10.21467/anr.6.1.11-28
ISSN: 2581-5164
RESEARCH ARTICLE

Temperature Dependence on Structural Properties of Liquid Phase Synthesized ZnO

Nii Abekah Akwetey Armah[1, 2*], Hubert Azoda Koffi[1]
[1]Department of Physics, University of Ghana, Legon, LG 63, Accra, Ghana
[2]Foundation Department, Lancaster University Ghana, P. O. Box CT9823, Cantonments, Accra, Ghana
[*]Corresponding Author email: akweteyniiabekah@gmail.com

Received: 28 October 2022 / Revised: 23 March 2023 / Accepted: 29 March 2023 / Published: 06 April 2023

ABSTRACT

Transparent conducting oxide material, ZnO nanoparticles has been synthesized using inexpensive and eco-friendly synthesis procedures with less or environmental pollutants and no liquid waste products. The effect of the temperatures on the structural properties for the synthesized ZnO nanocrystals has been investigated. In this study, we report an easy, low-cost, re-producible method for synthesizing ZnO nanoparticles by means of the liquid phase method. The ZnO nanocrystals were synthesized using the wet chemical route and the effect of temperature variation on the structural properties of investigated synthesized using powder x-ray diffractogram (XRD). The temperatures for the synthesis were varied from 120 °C to 200 °C in steps of 20 °C. The results show that, during the first stage of the synthesis of ZnO (at 120 °C), the XRD diffraction pattern confirms the cubic structure of zinc peroxide and the XRD pattern of the samples obtained at temperatures of 140 °C, 160 °C, 180 °C and 200 °C were confirmed to be hexagonal (wurtzite) crystal structure of ZnO. The XRD diffraction patterns of the 140 °C and 160 °C samples show some impurity phases which were associated with the zinc acetate by-product which is a colloid complex of water and methyl succinate and were removed by evaporation as temperatures were increased to 180 °C and 200 °C respectively. As temperature increases, the peak of the diffractograms of the sample becomes sharper and narrow indicating a decrease in width. A shift in peak positions to higher angles was observed and the positional parameter, bond angle, β, average crystallite size, APF, number of unit cells and density generally increase with temperature. However, the lattice parameters 'a' and 'c', bond lengths *b* and b_1, bond angle, *a*, dislocation density, strain and unit cell volume were found to generally decrease with temperature. The specific surface area was observed to generally decrease from 140 °C to 180 °C but suddenly increase sharply at 200 °C.

Keywords: Synthesis, ZnO, Temperature

1 Introduction

In a world where our dependence on most natural resources is almost always growing, it is important to research into new technologies which can sustain our needs without the use of non-renewable resources [1]. Nanotechnology is among the modern technologies which are creating waves in modern times. This is as a result of Louis Brus demonstration in 1984 that quantum confinement of the photo created electron-hole pair leads to the observed size dependent optical properties of nanocrystals. With the advancement in the development of nanotechnology, the nano-revolution is witnessing an explosion of research in diverse fields. This is made possible by metal oxide semiconductor nanocrystals also known as quantum dots [2].

Among the nanomaterials with industrial relevance and from all the transparent conducting oxide (TCO) materials considered, zinc oxide (ZnO) stands out as one of the most hopeful alongside Indium oxide (In_2O_3) and tin oxide (SnO_2) whether pure or doped [3]. ZnO has been a focus of interest for scientists and industry for decades and has been used for pigments and protective coatings on metals, but recent interest is because of its electrical and optical properties. ZnO nanoparticles have attracted increasing attention recently as alternate materials to indium tin oxide (ITO) because of the abundant, inexpensive and above all non-toxicity of Zn when compared with most currently used TCO materials [3], [4]. Due to its non-toxicity, it is a bio-safe and a bio-compatible material and consequently is being used for numerous biomedical applications such as biomedical implants, drug carriers, cosmetics and fillings in medical materials and several wide range medical applications [5], [6].

The importance of ZnO is owed to its unique chemical stability, physical, mechanical and thermal properties, highly efficient UV emission, high excitation binding energy of 60 MeV, high optical transparency in the visible region, low electrical resistivity, eco-friendly nature and above all its low cost make it a prospective candidate for industrial and other technological applications [7], [8], [5].

ZnO also stands out from other materials because of its ability to operate in tremendous conditions such as found in nuclear reactors and in space, due to its superior radiation hardness and high thermal conductivity than the majority of other materials [5]. Interesting applications of ZnO includes transparent electrodes, thin-film transistors, light-emitting diodes, ultraviolet laser diodes and photodetectors, solar cells, gas sensors, piezoelectric nanogenerators, spintronic devices and surface acoustic wave device [9], [8], [3].

In the advent of nanotechnology, several methods have been developed for the preparation of nanomaterials (particularly ZnO) [7], [8], [3] [10]. These are classified according to the medium of preparation as solution or liquid phase, solid phase and vapour phase methods [6]. Meanwhile, the production of these materials has been accomplished at a high price, with the primary challenges presently faced being the high cost of labourers and instruments, high temperature reaction and duration conditions, and an excess in generated waste.

The need to develop eco-friendly synthesis procedures for the production of nanoparticles arises as a result of recent nanotechnology research. Synthesis procedures are either expensive or they produce environmental pollutants. Many groups have focused on synthesis using the solution method. However, this leads to the production of liquid waste products. Another challenge associated with such synthesis procedures is the cost of energy due to heating for a long period of time and the need to work at very high temperatures. In this study, the focal point lies on the determination of optimum conditions for the synthesis of ZnO nanocrystals by the liquid phase method at utmost temperatures of 200 °C and to investigate the effect of the temperatures on the structural properties by powder x-ray diffractometer (XRD).

2 Methodology

2.1 Experimental Procedures

The chemicals and reagents that were used in the preparation of the samples for this experimental study were obtained from Maalab Scientific Equipment PVT, Ltd, Madhura Nagar, India. These are acetone, 99%; hydrogen peroxide, 30%; methanol, 99%; ethanol, 96% and zinc acetate dehydrate, 98.50%.

In this work, ZnO nanoparticles were prepared by grinding an amount of 3.292 g zinc acetate in an agate mortar with pestle and poured into a beaker containing an amount of methanol (40 ml) to dissolve. This was placed in a sonicator and sonicated for about 20 minutes till all the solute was dispersed. During the sonicating process drops of hydrogen peroxide (2 ml) were injected into the solution using a disposable syringe. The sonicating process was carried out to get the solute in the solution homogenized. The resulting solution became transparent when the zinc acetate was fully dispersed. All these processes were carried out at room temperature of (25±2) °C. The reaction mixture was transferred to a hot plate and heated slowly

to temperature range between 55 °C and 64 °C and maintained at this temperature for about 2 hrs. for complete dissolution of precursors and until all fluid was evaporated. This was to ensure that the solution did not boil since the boiling point of methanol is 65 °C. A gel was obtained. The temperature was then raised and held at 120 °C until the gel dehydrated and solidified into white crystals. Oxides are formed during hydrolysis and condensation of the dissolved species according to the following reaction:

$$Zn(CH_3COO)_2{\bullet}2H_2O + CH_3OH + H_2O_2 \rightarrow CH_2(CH_3COO) + ZnO_2 + 2H_2O + H_2 + 1/2O_2$$

Thus,

$$\begin{array}{l} H_2C\text{-}COOH \\ | \\ H_2C\text{-}COOCH_3 \end{array} + ZnO_2 + 2H_2O + H_2 + 1/2O_2$$

The white crystals were then cooled and ground. They were then returned to the hot plate at temperatures starting from 120 °C and gradually increasing to 140 °C within 10 mins and maintained at this temperature for about one and half hours till the colour changed from white to yellowish white. This was done in order to complete thermal decomposition of the initial precursors. During drying, complete conversion of ZnO_2 into ZnO occurred and was observed as a colour change. The decomposition of ZnO_2 was according to the equation:

$$ZnO_2 \rightarrow ZnO + 1/2O_2$$

The entire procedure was repeated three times at decomposition temperatures of 160 °C, 180 °C and 200 °C for each case. This procedure has been reported earlier in the work of Armah et al [11].

2.2 Structural Characterization

The crystal structure of the as prepared nanocrystals samples was studied using XRD. The powder XRD analysis was carried out using an X-ray powder diffractometer (PANalytical) with scintillation counter and monochromated CuKα (λ = 1.54056 Å) radiation. A 2θ scanning range from 20° to 70° was examined using a step size of 0.0060 and scan step time of 0.7 s and measuring temp of 25 °C.

Values of lattice parameters *a* and *c* were derived from equation 1 [12], [13] [14], [15]:

$$\frac{1}{d^2} = \frac{4}{3}\left[\frac{h^2+hk+k^2}{a^2}\right] + \frac{l^2}{c^2} \quad (1)$$

where *d* is the lattice plane spacing and *h*, *k*, *l* are the Miller indices.

The positional or internal parameter, u which is a measure of the amount by which each atom is displaced with respect to the next along the 'c' axis is determined by equation 2 [7], [14], [16], [17]:

$$u = \frac{a^2}{3(c)^2} + 0.25 \quad (2)$$

The nearest-neighbor bond lengths along the c-direction (expressed as *b*) and off c-axis (expressed as $b_1 = L$) can be calculated as follows [18], [19], [20]:

$$b = cu \quad (3)$$

$$b_1 = L = \sqrt{\frac{1}{3}a^2 + \left(\frac{1}{2} - u\right)^2 c^2} \quad (4)$$

The bond angles, α and β, are given by [3], [21], [22]:

$$\alpha = \frac{\pi}{2} + arccos\left[\left(\sqrt{1 + 3\left(\frac{c}{a}\right)^2\left(-u + \frac{1}{2}\right)^2}\right)^{-1}\right] \quad (5)$$

$$\beta = 2arcsin\left[\left(\sqrt{\frac{4}{3}+4\left(\frac{c}{a}\right)^2\left(-u+\frac{1}{2}\right)^2}\right)^{-1}\right] \quad (6)$$

The average crystallite size is determined from the full width at half maximum (FWHM) of the most intense diffraction line by using Debye- Scherrer equation:

$$D = \frac{K\lambda}{\beta Cos\theta} \quad (7)$$

where D is the particle size in nm, k is a constant of value 0.9, λ is the X-ray wavelength in nm, θ is the Bragg's angle in radians, and β is the full width at half maximum of the peak in radians [12], [17], [23].
The dislocation density (δ), which is the number of defects in the sample is calculated using equation 8 [7], [8], [14], [24];

$$\delta = \frac{1}{D^2} \quad (8)$$

where D is the crystallite size.
The strain, ε, induced in the as-prepared samples due to crystal imperfection and distortion was calculated using equation 9 [3], [12], [13], [25]:

$$\varepsilon = \frac{\beta}{4\,tan\theta} \quad (9)$$

The volume of the unit cell, V, is obtained from equation 10 [12] [26], [27]:

$$V = \frac{\sqrt{3}}{2}a^2c = 0.866a^2c \quad (10)$$

The number of unit cells (n) in the particle is calculated from equation 11 [3], [15]:

$$n = \frac{4}{3}\pi\left(\frac{D}{2}\right)^3\frac{1}{V} = \frac{\pi D^3}{6V} \quad (11)$$

Atomic parking fraction (APF) was calculated using equation 12 [27], [28]:

$$APF = \frac{2\pi}{3\sqrt{3}}\left(\frac{a}{c}\right) \quad (12)$$

The specific surface area (Sa) was determined from particle size of the ZnO nanoparticles using equation 13 [3], [24]:

$$S_a = \frac{6}{\rho \times D} \quad (13)$$

where D is the crystallite size and ϱ, the density of the ZnO, is computed with aid of equation 14 [3] [14]:

$$\rho = \frac{ZM}{N_A V} \quad (14)$$

where Z is the number of formula units in the unit cell (ZnO is 2), M is the molecular weight of the substance (ZnO=81.4 g/mol), N_A is Avogadro's number and V is the unit cell volume of the synthesized nanoparticles determined.

3 Results and Discussion

Characterization was done first on the zinc acetate used as the precursor and then on the prepared ZnO nanoparticles samples. In order to establish the most suitable temperature for which ZnO nanocrystals can be obtained in this study and to investigate the effect of temperature, the temperature was varied as 120 °C, 140 °C, 160 °C, 180 °C and 200 °C and corresponding effect in properties of the obtained particles were determined. The results for the structural properties are studied under peak indexing or phase

determination, particle size, lattice parameters (*a, c*), d-spacing, etc. The samples were scanned over 2θ values from 20◦ to 70◦.

3.1 Peak Indexing (Phase Determination)

The figure 1 below shows the diffractogram of the zinc acetate dehydrate used for this work. It can be seen that majority of the peaks are observed between 20° and 60° of 2 theta (degree). The three most prominent peaks are at 22.3°, 25.1° and 27.4°.

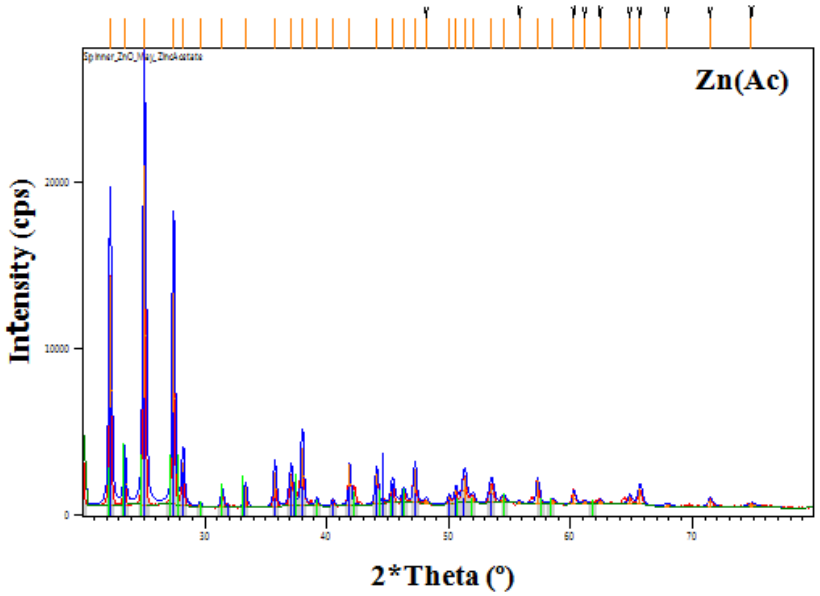

Figure 1: *Diffractograms of samples of pure zinc acetate nanoparticles*

The XRD diffraction pattern of the zinc acetate is confirmed by the Inorganic Crystal Structure Database (ICSD) scientific manual card number 00-033-1464 and is supported by [29], [30].
Figure 2 is the diffractogram obtained during the first stage of the synthesis of the ZnO prepared at 120 °C. At this temperature, the sample was found to be zinc peroxide (ZnO_2).

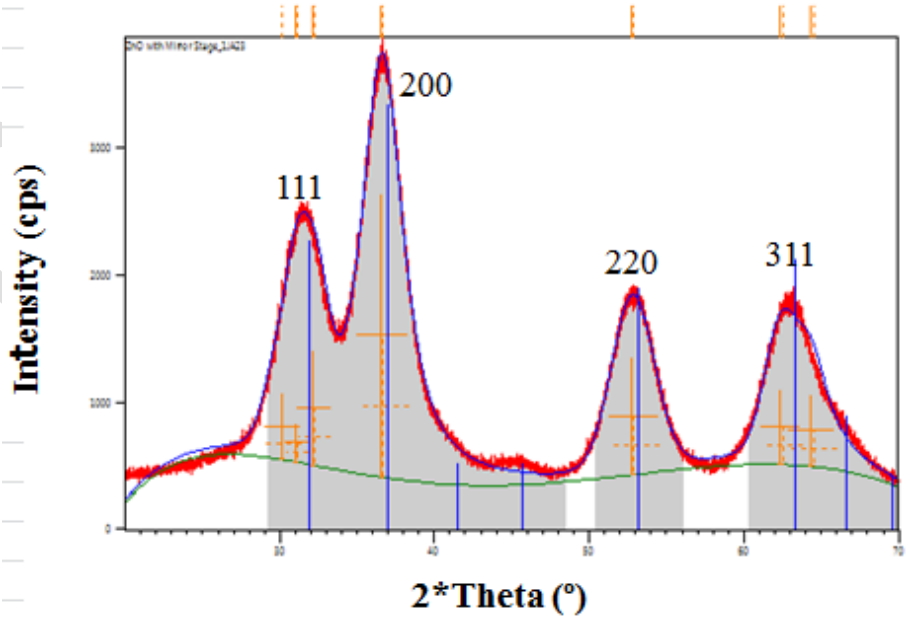

Figure 2: *Diffractogram of pure ZnO_2 nanoparticles at 120 °C*

The peaks are observed at 31.5445º, 36.6256º, 52.8603°, and 62.8293º corresponding to reflections from the planes (111), (200), (220) and (311). The XRD diffraction pattern of the ZnO_2 shown in Figure 2

confirms the cubic structure according to ICSD card number 00-013-0311. All the observed diffraction peaks of this work match with reported results of [31], [32] for cubic zinc peroxide with JCPDS card No. 13-0311 using the same zinc acetate dehydrate and hydrogen peroxide (30%) for synthesis.

The XRD pattern of the samples obtained at temperatures of 140 °C, 160 °C, 180 °C and 200 °C are presented in figure 3 (a-d). From the XRD it can be seen that the ZnO_2 decomposed into ZnO, and crystallinity improved as the temperature was increased. Additionally, the distinctive peaks got higher and sharper, indicating an enhancement of crystallinity nature due to agglomeration [14].

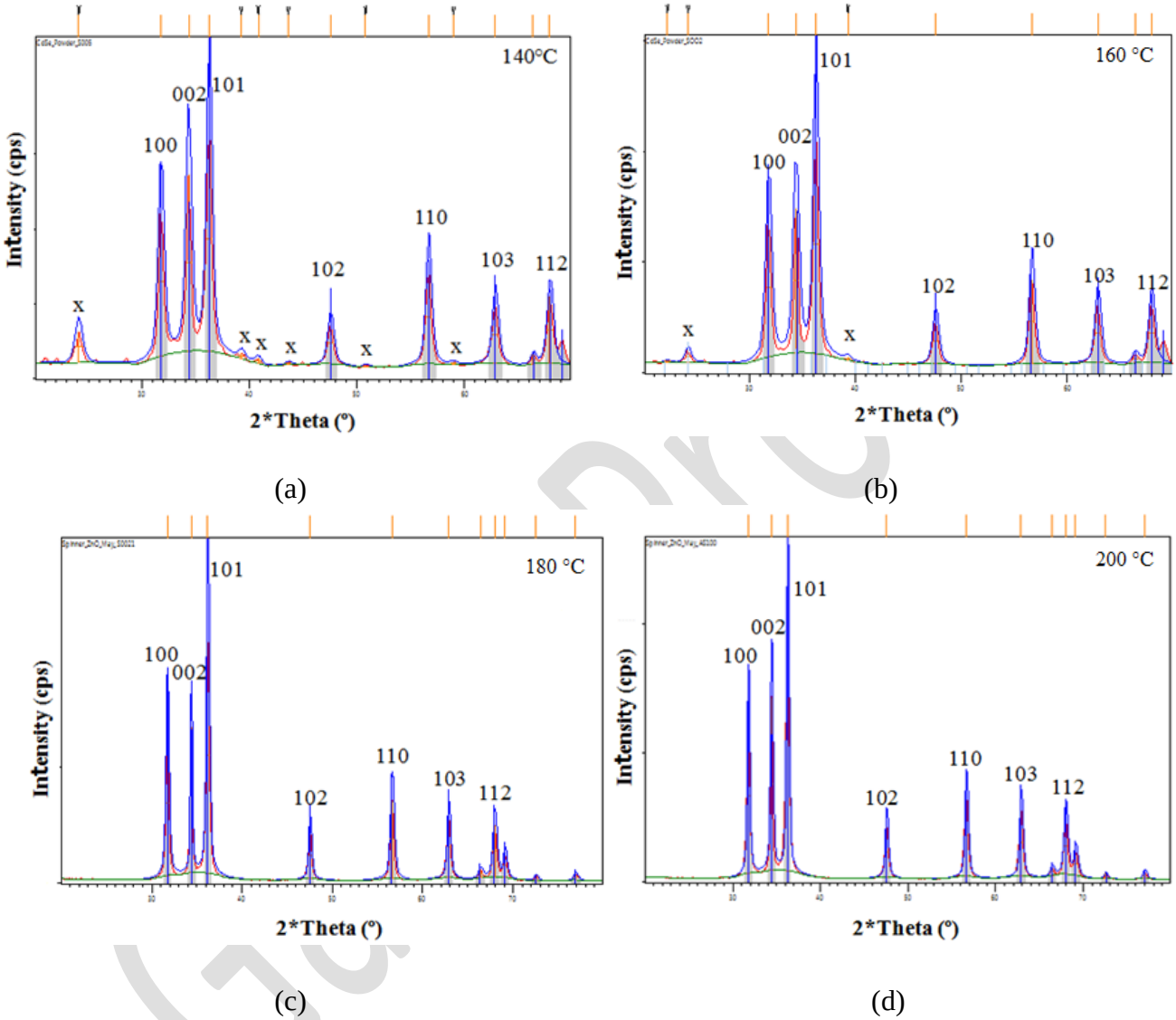

Figure 3: *Diffractograms of samples of pure ZnO nanoparticles obtained at temperatures of* **(a)** *140 °C* **(b)** *160 °C* **(c)** *180 °C and* **(d)** *200 °C.*

Peak indexing shows that samples prepared at 140°C and 160°C produced planes at (100), (002), (101), (102), (110), (103) and (112) at peak positions (2θ values) of approximately 31.76°, 34.31°, 36.22°, 47.52°, 56.63°, 62.83° and 67.92° which were found to be ZnO and confirms the hexagonal wurtzite structure accordingly. With reference to the sample synthesized at 140 °C (figure 3a), it could be observed that, in addition to the reflections from planes indexed to ZnO, there are additional unidentified peaks with low intensity at approximately 24.10°, 39.22°, 40.78°, 43.60°, 50.78° and 58.95° indexed as 'x'. With reference to the sample synthesized at 160 °C as shown on figure 3(b), after peak indexing, there were still additional peaks at approximately 24.17° and 39.27°. All the additional peaks indexed as 'x' could be traced to the diffractogram of the zinc acetate which is also confirmed by [30]. They could also be attributed to the zinc acetate by-product which is a colloid complex of water and methyl succinate and is expected to be removed

by evaporation. It is interesting to note that, these additional peaks have also been observed by [33] at a similar position even though in their work, the precipitates of the samples were filtered and washed several times to remove starting material before drying. A study from [34] also shows that the extra peaks possibly originate from the presence of residual in volatile organic compounds resulting from incomplete decomposition of the metal-organic source of the zinc acetate. However, by increasing the synthesis temperature to 180 °C (Figure 3c) and then to 200 °C (Figure 3d) no extra peaks relating to the impurities were observed, signifying that the final product is exclusively ZnO nanostructures. Thus, the additional peaks disappeared while the ZnO peaks triumphed. All the observed peaks correspond very well with the reference data to ICSD card numbers 01-073-8765 and 01-078-2585 respectively for the wurtzite structure of ZnO.

3.2 Peak Positioning

In all the four diffractograms, the most dominant or prominent peak was observed to be the (101) plane at approximately 36.2°. At temperature of 140 °C, it is observed that the ZnO nanoparticles exhibit strong (002) orientation than the (100). When the temperature increased to 160 °C, the preferred orientations changed from (002) to (100). At 180 °C both peaks were at the same height but at 200 °C the orientations changed again from (100) to (002). It is therefore clear that as temperature is increased the nanoparticles adopt a preferred orientation, with the c-axis at (002). This could be as a result of different morphology of nanoparticles, which are dependent on the temperature which affects the geometry of the aggregates [34]. The increase in temperature is likely to drive the modification of the grain boundary configuration during growth, which accompanies the appearance of new crystal grains. This trend has been supported by [35]. Additionally, it was observed that, as temperature increases, the peak of the diffractograms of the sample becomes sharper and narrow, thus width decreases. This type of result has also been reported by [36], [37]. The general trend in peak positions, is that as temperature increases, there is a corresponding increase in peak positions. Thus, a shift to higher angles (right shift). This implies that a slight variation in the lattice parameters occurs as growth temperature increases, attributable to a change in the stress in the ZnO nanoparticles. This type of result in the shift of peak position angle to higher values has also been reported by [14], [15]. This is shown in Figures 4 (a), (b) and (c), for the (100), (002) and (101) planes respectively.

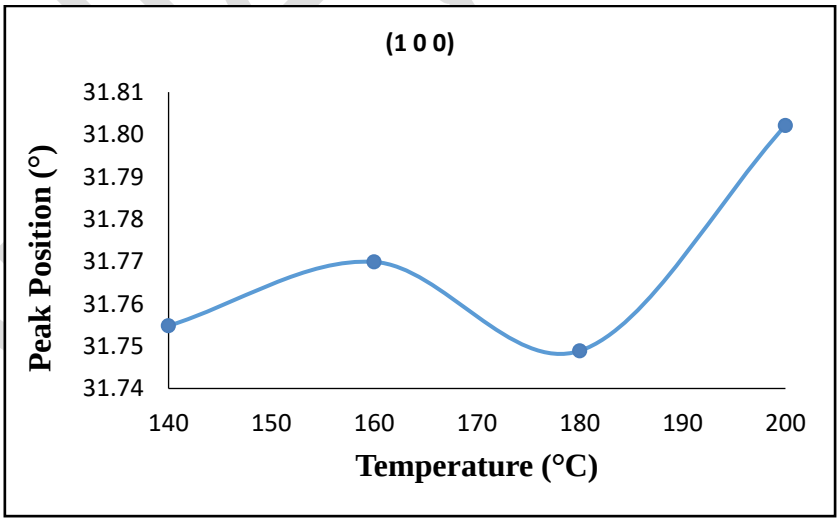

(a)

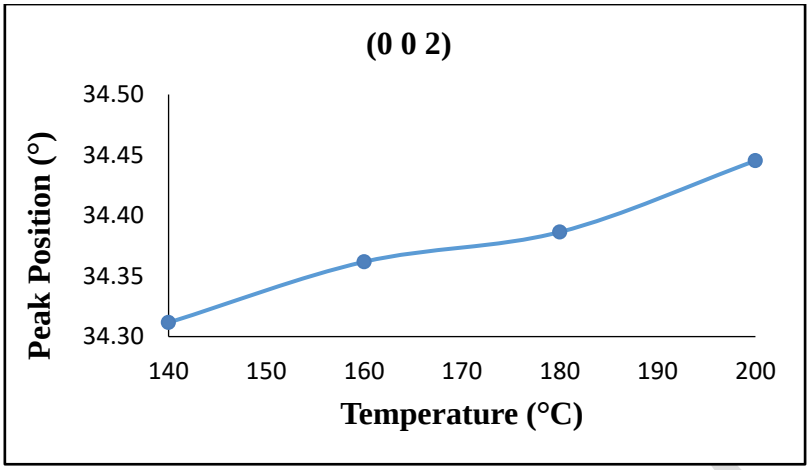

(b)

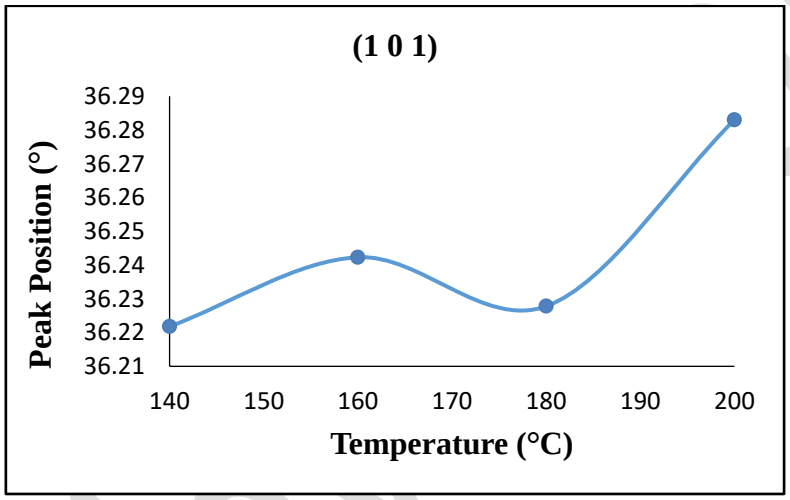

(c)

Figure 4: *Peak position versus temperature for ZnO nanoparticles*

3.3 Lattice Parameters (a, c)

The lattice parameters, *a* and *c* were plotted against the temperatures as shown in figure 5.

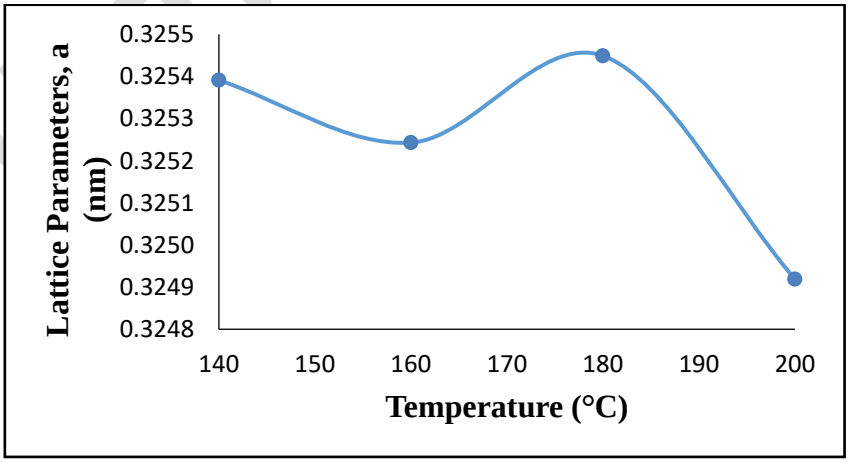

(a)

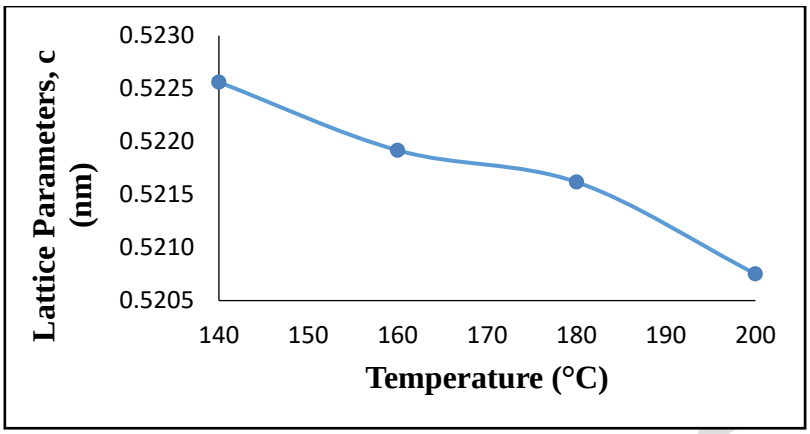

(b)

Figure 5: *Lattice parameters, a and c versus temperature for ZnO nanoparticles*

The lattice parameters, *a,* decreased slightly from 140 °C to 160 °C and then increased sharply at 180 °C before decreasing again sharply at 200 °C. For the lattice parameters, *c,* the decrease was even and gradual throughout as observed in figure 5. Thus, whiles the trend for the lattice parameter a looks fluctuating, that of the lattice parameter, *c,* decreased almost linearly as the temperature is increased and decreased to a minimum at the highest temperature of 200 °C. It can be said that, generally, as the temperature is increased, the lattice parameters, *a*, and *c* decreased. The trend of the decrease in the value of the lattice parameters is supported by [14], [38] [39]. The values of the lattice parameter were found to be close to those of the standard ZnO from the ISCD cards 01-073-8765 and 01-078-2585 (3.2533 - 3.2522 and 5.2072 - 5.2095). However, there were slight differences as temperature was varied and this accounted for the small expansion and contraction in the crystal lattice of the ZnO and confirms the small shift in the XRD diffraction peaks. The observation of small differences in the lattice parameters values, which could be attributable to calcination temperature confirms the presence of point defects and oxygen vacancies [14]. The expansion of lattice due to increased growth temperature is responsible for the increase in lattice parameters 'a' and 'c' [15].

3.4 The Positional or Internal Parameter

From figure 6, it can be observed that the positional parameter increased sharply with temperature from 140 °C to 160 °C and continue to increase further to 180 °C and then remain virtually stable from 180 °C to 200 °C with just a slight increase. The minimum value is 0.37925 which is observed at 140 °C and the maximum is observed at 200 °C with a value of 0.37977. This value is supported by [14]

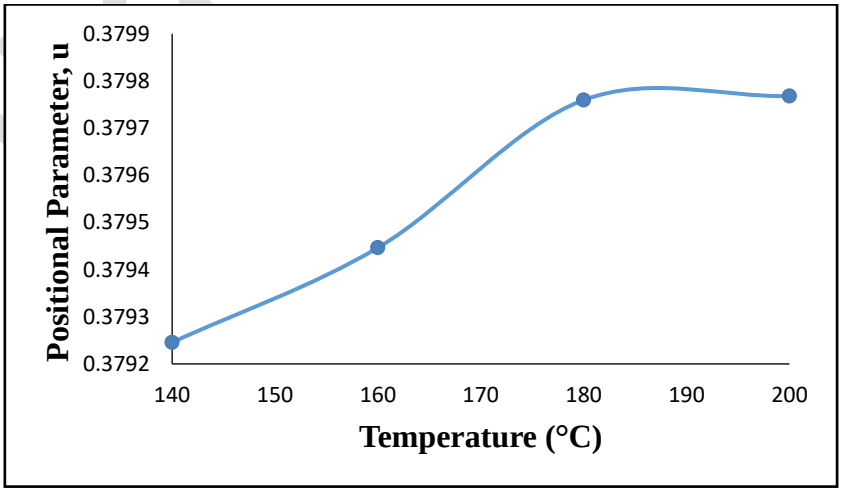

Figure 6: *Positional parameter of ZnO nanoparticles versus temperature*

3.5 Bond Lengths

Figures 7 and 8 show plots of the two Zn–O bond length, that nearest-neighbor bond lengths along the c-direction (expressed as b) and off c-axis (expressed as $b_1 = L$) as against the variation in temperatures respectively. It can be observed that, generally, both bond lengths decreases as temperature is increased. From figure 7, it can be observed that the bond length along the c-direction, b, decreased slightly from 140 °C to 160 °C and then increased slightly from the 160 °C to the 180 °C before decreasing again drastically from 180 °C to 200 °C. The trend shows a general decrease in value as temperatures increase. According to this study, the values of the bond length b, range between 0.197765 being the minimum at 200 °C and 0.198179 the maximum at 140 °C. This value is supported by [14].

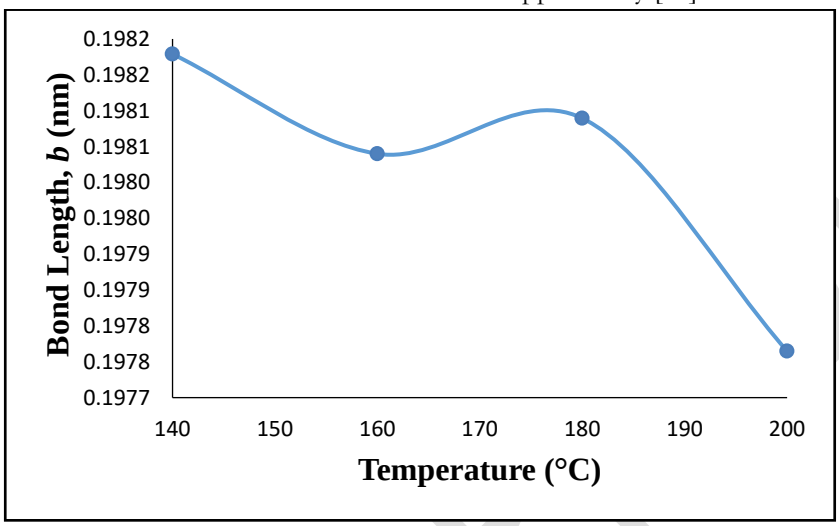

Figure 7: *Bond length b versus temperature for ZnO nanoparticles*

The bond length off c-axis, b_1, shown in Figure 8 also shows a similar trend but with an exception. Thus, instead of an increase in bond length from the 160 °C to the 180 °C as with the b, the bond length rather decrease slightly almost in the form of linearity. The values of the bond length, b_1, calculated according to this study, range between 0.260256 and 0.261012 nm. With reference to both bond lengths, it was found that the b_1 values are higher than that of the b.

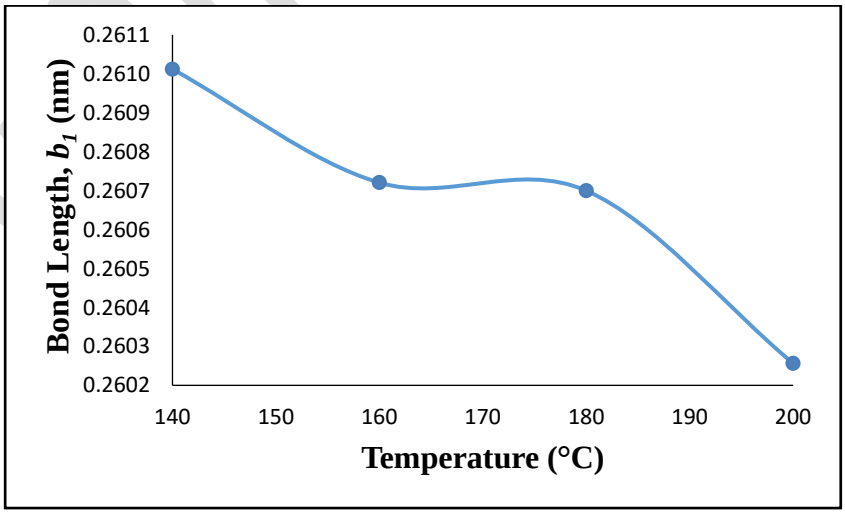

Figure 8: *Bond length b_1 versus temperature for ZnO nanoparticles*

3.6 Bond Angles

Figures 9 and 10 shows a plot of the two bond angles, α and β, as against the variation in temperatures respectively. It can be observed that, generally, bond angle, α decreases as temperature is increased whiles the bond angles, β, increases as temperature is increased.

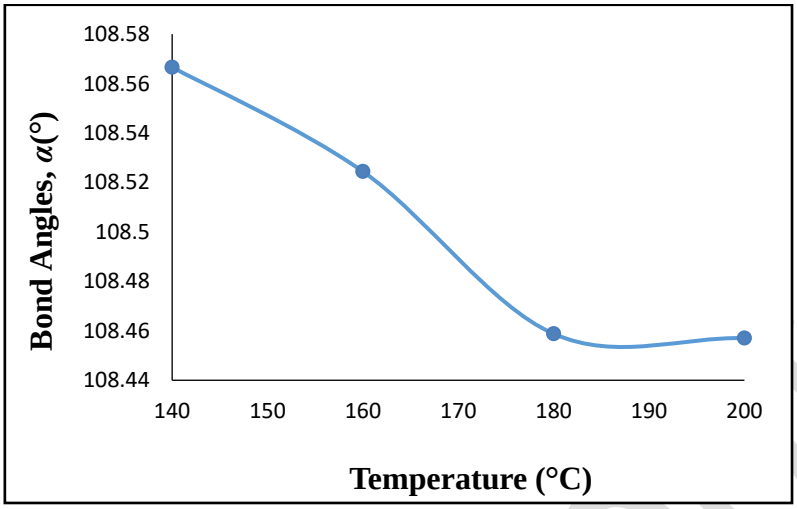

Figure 9: *Bond angle, α, versus temperature for ZnO nanoparticles*

From figure 9, it can be observed that the bond angle, α, decreased slightly linearly from 140 °C to 160 °C and then decreased drastically from the 160 °C to the 180 °C before further decreasing slightly linearly at the temperature of 200 °C. The values of the bond angle, α, range between 108.457 and 108.567with the lowest at 200 °C and highest at 140 °C. With reference to Figure 10, the bond angle, β, shows an opposite trend. It can be observed that the bond angle, β increased sharply with temperature from 140 °C to 160 °C and continue to increase further to 180 °C and then remain almost stable from 180 °C to 200 °C with just a slight increase. The minimum value is 110.36 which is observed at 140 °C and the maximum is observed at 200 °C with a value of 110.47. With reference to both bond angles, the angle, β, was found to be higher than that of angle, α. This value is supported by [14].

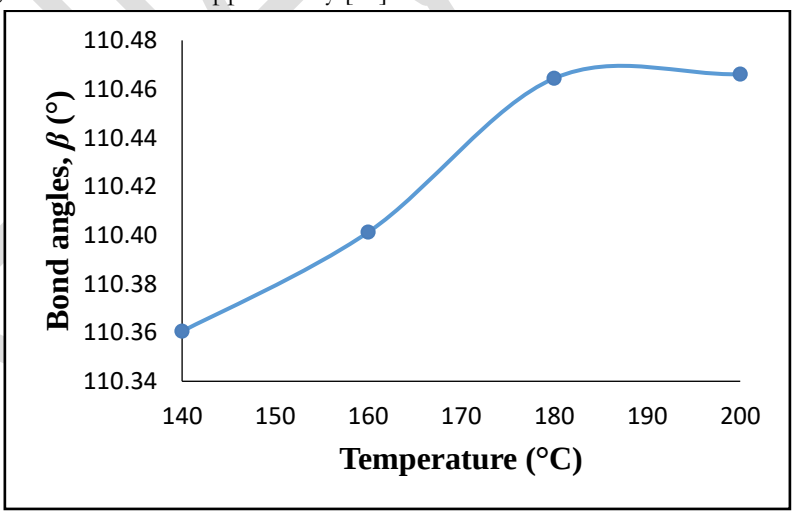

Figure 10: *Bond angle, β, versus temperature for ZnO nanoparticles*

3.7 Average Crystallite Size

From Figure 11, it can be observed that the average crystallite size increased slightly beyond the 140 °C at 160 °C and then increased sharply from the 160 °C to the 180 °C before decreasing at the 200 °C. However, it can be said that, generally there is an increase in the average crystallite size as the temperature is increased

even though the trend is fluctuating. This is supported by the fact that the crystalline nature of the ZnO nanoparticles decreases with increasing temperatures from 140 °C to 200 °C, as is indicated by sharp peaks. The maximum crystallinity is observed at 140 °C, while the samples at 180 °C have the lowest crystallinity. The value is in the range of 14.89 nm to 23.22 nm. This result is supported by [40] who argues that the possibility of fusion of grain boundaries resulting in a marginal increase in particle size cannot be ruled out at increasing temperature. Other researchers whose work support this trend are [41], [25] [42] [43].

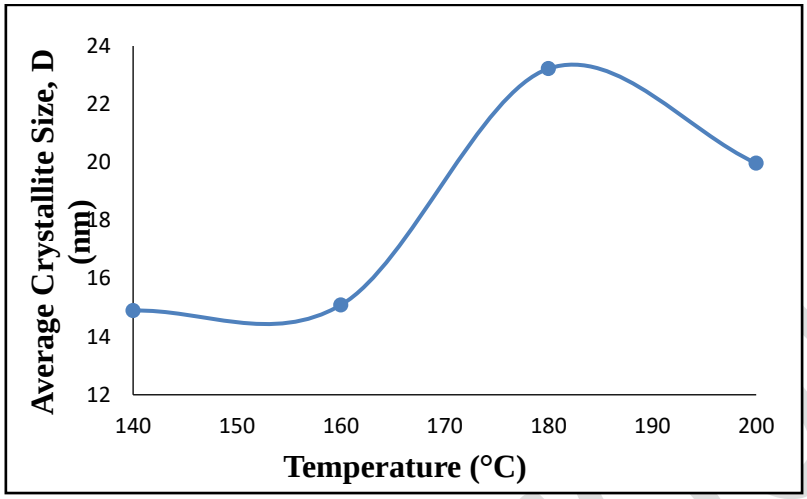

Figure 11: *Average crystallite size versus temperature for ZnO nanoparticles*

The increase in crystalline size values with an increase in temperature is attributed to the enlargement of grain sizes and a decrease in the micro strain while increase in dislocation density [8]. This could also be linked to an increase in crystal growth rate as a result of volume expansion and a decrease in system supersaturation at high temperatures [14]. Kaningini et al [42] suggested that higher annealing temperatures improve the crystal quality of the ZnO nanoparticles inducing a reduction of the full-width half-maximum value. The growth in the particle size could also be attributed to smaller particles agglomerating or amalgamating into larger particles, which is a result of solid-state diffusion which is an atomic migration from one point to another through the solid [43].

3.8 Dislocation Density

Figure 12 shows a plot of dislocation density as against the variation in temperatures. It can be observed that, the dislocation density decreases as the temperature increases from 140 °C to 180 °C and increase slightly at 200 °C. The lowest value is at a temperature of 180 °C with the highest at 140 °C. The decrease in the dislocation density indicates a decline in the number of defects or the length of dislocation per unit volume in the nanocrystals sample synthesized which is as a result of strain [25], [5], [14].

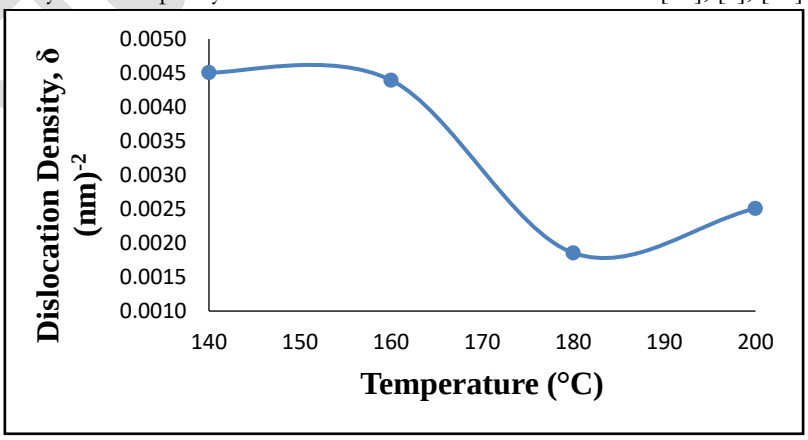

Figure 12: *Dislocation density versus temperature for ZnO nanoparticles*

The observed trend in the dislocation density can be said to generally decrease as temperature increase irrespective of the rise in value at 200 °C. The decrease in the dislocation density signifies a decline in crystallography deformation, topological imperfection or irregularity [44], [24]. The lower values of dislocation density are attributed to the lower level of the defect and better crystalline quality of the ZnO sample at higher temperature. This trend of results is in good agreement with the work of [25], [5], [14].

3.9 Wilson Lattice Strain

The strain determined by the method given in equation 9 resulted from induced line broadening. The plot below shows a trend of negative strain in terms of the slope.

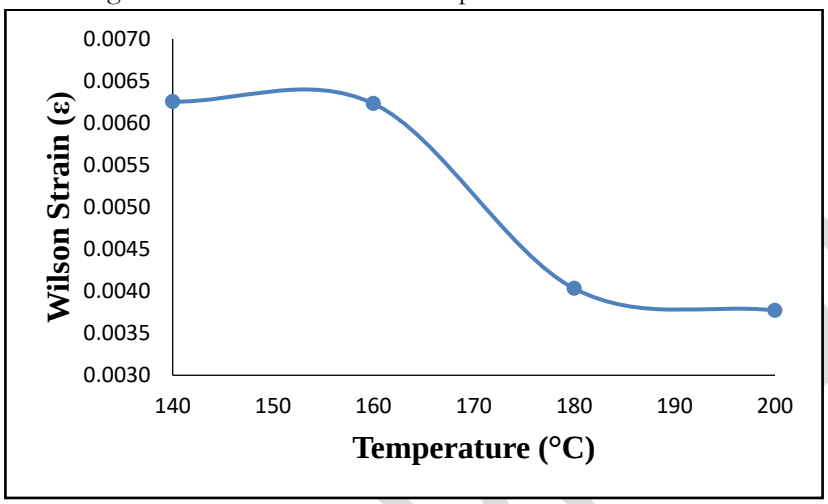

Figure 13: *Strain versus temperature for ZnO nanoparticles*

From Figure 13 shown below, it can be observed that the strain decreased slightly from 140 °C to 160 °C and then decreased drastically from the 160 °C to the 180 °C before further decreasing slightly again at the temperature of 200 °C. The trend in the strain results shows a decrease in value as temperatures increase. The strain values range between 0.003771 and 0.006254 with the lowest at 200 °C. Similar trend in the decrease in strain is reported by [45]. This strain may be due to the lattice shift and shrinkage that was observed in the lattice parameters [46].

3.10 Volume of Unit Cell

Figure 14 shows that the volume of the unit cell decreased beyond the 140 °C at 160 °C and then suddenly increased slightly from the 160 °C to the 180 °C before further increasing again sharply at the temperature of 200 °C.

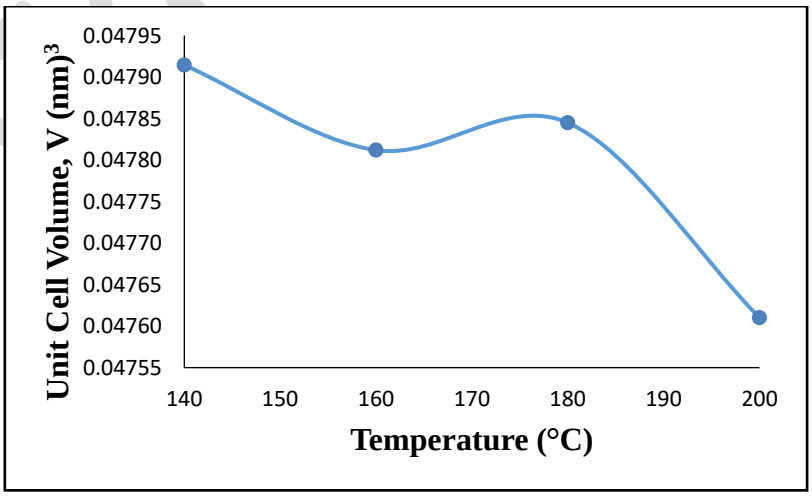

Figure 14: *Volume of the unit cell versus temperature for ZnO nanoparticles*

Generally, there is a decrease in the volume of the unit cell as the temperature is increased even though the trend is fluctuating. The values of the volume of the unit cell were found to be between a minimum 0.04761 at 200 °C and maximum of 0.04791 at 140 °C with an average of approximately 0.0478. This value is supported by [3]. The values were slightly higher than that of the standard ZnO from the ISCD which is 0.04773 nm^3. This result could be attributed to the lattice parameters. Other reasons for the difference could be related generally to the method of synthesis, which depends on external and environmental factors such as the type and source of precursor, temperature, time, and impurities [47]. The graph demonstrates that as the calcination temperature rises, the volume of the unit cell decreases. This trend is consistent with [11].

3.11 Atomic parking fraction (APF)

It can be observed from Figure 15 that the APF increases sharply with temperature from 140 °C to 160 °C and continue to increase further to 180 °C and then remain almost stable from 180 °C to 200 °C with just a slight increase. The maximum APF is observed at 200 °C with a value of 0.75457, while the minimum is observed at 140 °C with a value of 0.75305 with an average of 0.75. This value is supported by [3].

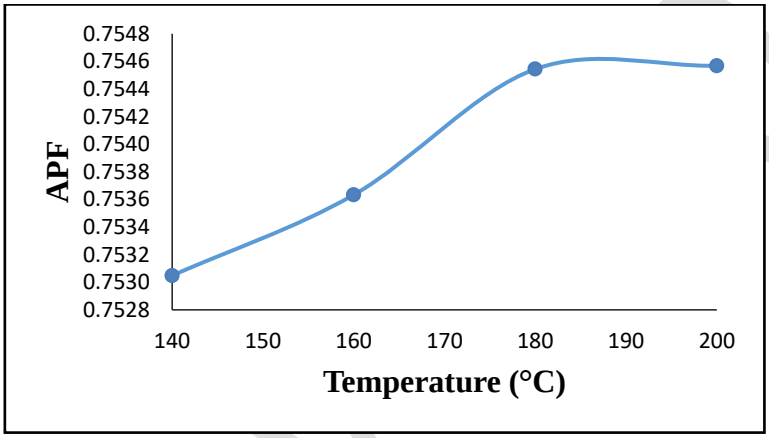

Figure 15: *APF versus temperatures for ZnO nanoparticles*

The APF of bulk hexagonal ZnO materials is about 0.74 but, in this study, the APF was 0.75 which is more than the value of the bulk material. This is attributed to the size effect in the nanocrystallite samples [44].

3.12 Number of Unit Cell, n

The number of unit cell obtained in this work as against the temperature variation is as plotted in Figure 16.

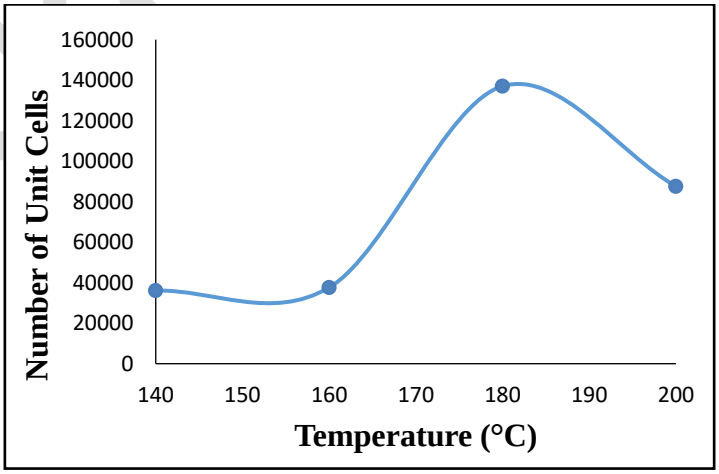

Figure 16: *Number of unit cell versus temperatures for ZnO nanoparticles*

It can be observed that as temperature increase from 140 °C to 160 °C, there was almost a constant value with slight increment. As the temperature increased, there was an increment from 160 °C to 180 °C and then a decrease at 200 °C. The trend can be said to be fluctuating. This variation could be attributed to average crystallite size and the volume of the unit cell as number of unit cell is dependent of these parameters.

3.13 Specific Surface Area (SSA)

It can be observed from Figure 17 that the specific surface area decreased sharply with temperature from 140 °C to 160 °C and further decrease slightly to 180 °C and suddenly increased sharply from 180 °C to 200 °C. The maximum specific surface area is observed at 140 °C, while the minimum is observed at 180 °C. This variation could be partly attributed to average crystallite size and the volume of the unit cell. The specific surface area decreases with increasing particle size since the relationship is inversely proportional. The decrease in the specific surface area also signifies less or reduced pores in the particles. A larger surface area signifies smaller particle sizes.

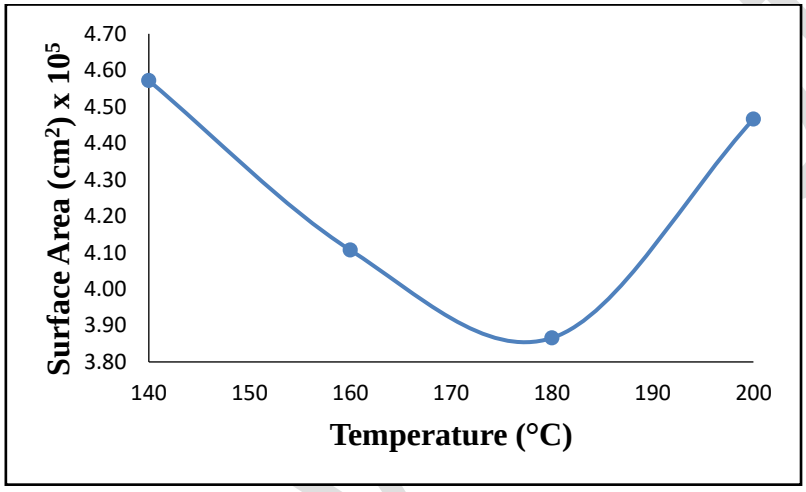

Figure 17: *Specific surface area versus temperatures for ZnO nanoparticles*

3.14 X-Ray Density

From Figure 18, it can be observed that the density increased beyond the 140 °C at 160 °C and then suddenly decreased slightly from the 160 °C to the 180 °C before further increasing again at the temperature of 200 °C. However, it can be said that, generally there is an increase in the density as the temperature is increased even though the trend is fluctuating.

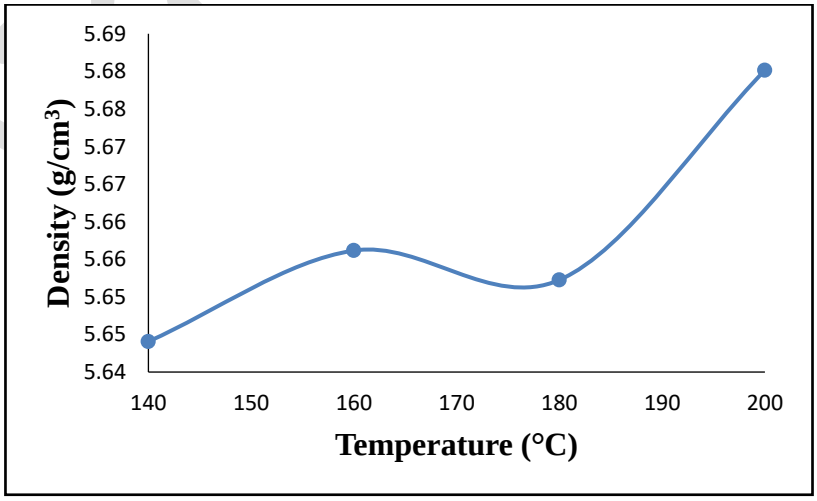

Figure 18: *Density versus temperature for ZnO nanoparticles*

The maximum density is observed at 200 °C, while the minimum is at 140 °C. The value of the density obtain is between 5.644 and 5.680 with an average of 5.658 which close to the standard value 5.65 from the ISCD card and in good agreement. This value is supported by [3].

4 Conclusions

The study has been carried out to synthesize zinc oxide particles through liquid phase method at varied temperatures of 120 ℃, 140 ℃, 160 ℃, 180 ℃ and 200 ℃ respectively. The results lead to the conclusion that zinc oxide have been successfully synthesized using a non-toxic, a low-cost, and eco-friendly precursors. X-ray diffraction analysis of the synthesized samples were conducted to identify their crystalline structure and phase purity and the effect of temperature. From the discussion, it could be concluded that during the first stage of the synthesis of ZnO (at 120 °C), the XRD diffraction pattern confirms the cubic structure of zinc peroxide. The XRD pattern of ZnO samples obtained at temperatures of 140 °C, 160 °C, 180 °C and 200 °C all confirms a hexagonal (wurtzite) crystal structure of ZnO. However, secondary phases from the XRD diffraction patterns were observed for the ZnO samples synthesis at 140 °C and 160 °C but not at temperatures of 180 °C and 200 °C. As temperature increases, the peak of the diffractograms of the sample becomes sharper and narrow, thus width decreases. Shifts in peak positions in the diffraction pattern due to increasing temperature have been observed generally to be at higher angles. The crystallite size confirms the synthesis of ZnO nanocrystals. The results of the lattice parameters 'a' and 'c', bond lengths b and b1, bond angle, α, dislocation density, strain and unit cell volume were found to generally decrease with temperature. That of the positional parameter, bond angle, β, average crystallite size, APF, number of unit cells and density generally increase with temperature. The specific surface area generally decreases from 140 °C to 180 °C but suddenly increase sharply afterwards up to 200 °C.

5 Declarations

5.1 Competing Interests

The author declares no conflict of interests.

5.2 Publisher's Note

AIJR remains neutral with regard to jurisdictional claims in institutional affiliations.

How to Cite this Article:

Will be updated in the final version.

References

[1] A. M. A. Lockett, "Novel Approach to the Deposition of ZnO Nanostructures for Use in Solar Cells", *PhD Thesis, University of Manchester*, 2011.

[2] S. J. Rosenthal, J. McBride, S. J. Pennycook and L. C. Feldman. "Synthesis, surface studies, composition and structural characterization of CdSe, core/shell and biologically active nanocrystals", *Surface Science Reports 62,* pp.111–157, 2007.

[3] A. Z. Mahmoud, E. M. M. Ibrahim, Lamiaa Galal, and E. R. Shaaban, "Influence of Fe Substitution on Structural Morphological and Magnetic Properties of Zn1-xFexO Thin Films to Various Applications", *Sohag J. Sci. 8(1), 91-98, 202*3 DOI: 10.21608/sjsci.2022.153658.1017

[4] S. K. Bajpai, V. Thomas and M. Bajpai. "Novel Strategy for Synthesis of ZnO Microparticles Loaded Cotton Fabrics and Investigation of their Antibacterial Properties", *Journal of Engineered Fibers and Fabrics, 6*(3), 2011.

[5] A. Anjum, R. Ahmed, Z.A. Umar, S. Azzam, T. Hussain, M.N. Sarwar and M.A. Baig, "Structure and defects-related optical properties of highly (002)-oriented zinc oxide thin films", *Physica* B 644, 2022. DOI: 10.1016/j.physb.2022.414195

[6] T. S. Sazanova, L. A. Mochalov, A. A. Logunov, M. A. Kudryashov, D. G. Fukina, M. A. Vshivtsev, I. O. Prokhorov, P. A. Yunin, K. A. Smorodin and A. A. Atlaskin. "Influence of Temperature Parameters on Morphological Characteristics of Plasma Deposited Zinc Oxide Nanoparticles". *Nanomaterials* 12, 1838, 2022, DOI: 10.3390/nano12111838

[7] M. Lal, P. Sharma and C. Ram, "Optical, structural properties and photocatalytic potential of Nd-ZnO nanoparticles synthesized by hydrothermal method", *Results in Optics* 10, 100371, 2023. DOI: 10.1016/j.rio.2023.100371

[8] B. Amudhavalli, R. Mariappan, and M. Prasath, "Low-cost nebulizer spray deposited conduction mechanism of thin film ZnO nanoparticles", *Journal of Ovonic Research*, Vol. 19, No. 1, p. 53 – 63, 2023. DOI: 10.15251/JOR.2023.191.53

[9] R. Yatskiv, J. Grym, N. Baˇsinov´a, ˇS. Kuˇcerov´a, J. Vaniˇs, L. Piliai, M. Vorokhta, J. Veselý and J. Maixner, "Defect-mediated energy transfer in ZnO thin films doped with rare-earth ions", *Journal of Luminescence*, 253, 119462, 2023. DOI: 10.1016/j.jlumin.2022.119462

[10] M. A. Gatou, N. Lagopati, I.-A. Vagena, M. Gazouli and E.A. Pavlatou. "ZnO Nanoparticles from Different Precursors and Their Photocatalytic Potential for Biomedical Use". *Nanomaterials*, 13, 122, 2023. DOI: 10.3390/nano13010122

[11] E. N. A. Armah, F. K. Ampong, M. Egblewogbe, H. A. Koffi, F. Boakye, J. K. A. Amuzu, R. K. Nkum, "Solubility of Mn in ZnO Nanocrystallites using Wet Chemical Synthesis", *Adv. Nan. Res.;* Vol. 2, no. 1, pp: 53-61, November 2019. DOI: https://doi.org/10.21467/anr.2.1.53-61

[12] V. Ganesh, B. R. Kumar, T. H. AlAbdulaal, I. S. Yahia, M. S. Abdel-wahab, R. Ade, M. S. A. Hussien and M. Keshway. "Electrocatalytic Degradation of Rhodamine B Using Li-Doped ZnO Nanoparticles: Novel Approach". *Materials*, 16, 1177, 2023. DOI: 10.3390/ma16031177

[13] G. Barsisa1, A. Belay, G. Beyene, C. Seboka and K. Gudishe, "Synthesis Europium (Eu3+) Doped Zinc Oxide Nanoparticles via the Co-Precipitation Method for Photocatalytic Applications", *Nano Biomed. Eng.*, Vol. 14, Iss. 1, 2022.

[14] A. M. Mohammad, H. S. Ahmed Al-Jaf, H. Sh. Ahmed, M. M. Mohammed, Z. T. Khodair, "Structural and morphological studies of ZnO nanostructures", *Journal of Ovonic Research*, Vol. 18, No. 3, p. 443–452, 2022, DOI: 10.15251/JOR.2022.183.443

[15] F. B. Dejene. "Characterization of low-temperature-grown ZnO nanoparticles: The effect of temperature on growth", *J. Phys. Commun*. 6, 075011, 2022. DOI: 10.1088/2399-6528/ac8049

[16] M. Amjad, M. I. Khan, N. Alwadai, M. Irfan, Ikram-ul-Haq, H. Albalawi, A. H. Almuqrin, M. M. Almoneef, and M. Iqbal. "Photovoltaic Properties of ZnO Films Co-Doped with Mn and La to Enhance Solar Cell Efficiency", *Nanomaterials*, 12, 1057, 2022. DOI: 10.3390/nano12071057

[17] D. Kumar and M. S. Mehata. "Synthesis of diamagnetic ZnO nano-crystallites via sol-gel method and their photocatalytic activity", *Indian Journal of Engineering & Materials Sciences*, Vol. 29, pp. 437-444, August 2022. DOI: 10.56042/ijems. v29i4.48695

[18] H. Morkoc. "Handbook of Nitride Semiconductors and Devices: Materials Properties", *Physics and Growth*, Vol.1, John Wiley and Sons, New Jersey, 2009.

[19] A. A. Othman, M. A. Osman, E. M. M. Ibrahim, M. A. Ali, A. G. Abd-Elrahim, "Mn-doped ZnO nanocrystals synthesized by sonochemical method: Structural, photoluminescence, and magnetic properties", *Materials Science and Engineering*, B 219, pp.1–9, 2017.

[20] C. Belkhaoui, N. Mzabi and H. Smaoui. "Investigations on structural, optical and dielectric properties of Mn doped ZnO nanoparticles synthesized by co-precipitation method", *Materials Research Bulletin 111*, Volume 2021, pp.70–79, 2019. doi.org/10.1155/2021/9926544

[21] H. Morkoç and Ü. Özg€ur, "Zinc Oxide: Fundamentals, Materials and Device Technology", WILEY-VCH Verlag GmbH & Co. KGaA, Weinheim, 2009.

[22] M. N. H. Mia, S. M. Rana, M. F. Pervez, M. R. Rahman, M. K. Hossain, A. A. Mortuza, M. K. Basher, M. Hoq. "Preparation and spectroscopic analysis of zinc oxide nanorod thin films of different thicknesses", *Materials Science-Poland*, Vol. 35, no.3, pp.501-510, 2017. DOI: 10.1515/msp-2017-0066

[23] M. Nabil, I. V. Perez-Quintana, M. Acosta, J. A. Mendez-Gamboa, and R. Castro-Rodriguez, "Morphological, Structural, and Optical Bandgap Characterization of Extracted ZnO Nanoparticles from Commercial Paste", *Advances in Materials Science and Engineering*, Volume 2021, pp.1-7, 2021. Doi.org/10.1155/2021/9926544

[24] E. A. Mohammed, "A comparative study of the method of Williamson Hall and the pattern of cadmium oxide nanoparticles for X-rays", *Turkish Journal of Computer and Mathematics Education* Vol.12 No. 4, pp.881-889, 2021.

[25] A. F. Abdulrahman, S. M. Ahmed, S. M. Hamad, and A. A. Barzinjy, "Effect of Growth Temperature on Morphological, Structural, and Optical Properties of ZnO Nanorods Using Modified Chemical Bath Deposition Method", *Journal of Electronic Materials*, Vol. 50, No. 3, 2021. Doi.org/10.1007/s11664-020-08705-7

[26] R. Kant, D. Sharma, A. Bansal and R. Singh. "Structural, optical and dielectric properties of Al/Mn doped ZnO nanoparticles, a comparative study", *Materials Technology*, Vol. 36, no.9, pp.513-520, 2021. DOI: 10.1080/10667857.2020.1775408

[27] S. M. Abdou and K. M. Al-mokhtar, "Synthesis and Characterization of Mn-Doped ZnO Nanoparticles and Effect of Gamma Radiation", *Arab J. Nucl. Sci. Appl*., Vol. 55, no.2, pp.53 -59, 2022.

[28] O. Bilgili, "The Effects of Mn Doping on the Structural and Optical Properties of ZnO", *ACTA Physica Polonica A*, Vol. 136, No. 3, 2019.

[29] A. P. Raj and C. R. Raja. "Synthesis, Growth, Structural, Spectroscopic, Thermal and Optical Properties of NLO Single Crystal: L-Threonine Zinc Acetate". *Photonics and Optoelectronics*, Vol.*2*, no.3, pp.56, 2013.

[30] C. M. Jay, M. Sathya, K. Pushpanathan "Effect of pH on Crystal Size and Photoluminescence Property of ZnO Nanoparticles Prepared by Chemical Precipitation Method" *Acta Metall. Sin. (Engl. Lett.)*, 28, pp.394-404, 2015.

[31] R. Esparza, A. Aguilar, A. Escobedo-Morales, C. Patiño-Carachure, U. Pal, G. Rosas and R. Pérez. "Synthesis of ZnO_2 Nanocrystals Produced by Hydrothermal Process", *Mitei. Res. Soc. Symp. Proc.* Vol. 1242, 2010.

[32] N. Singh, S. Mittal, K. N. Sood, Rashmi, and P. K. Gupta. "Controlling the Flow of Nascent Oxygen Using Hydrogen Peroxide Results in Controlling the Synthesis of ZnO/ZnO_2". *Chalcogenide Letters.* Vol.7, no.4, pp.275-281, 2010.

[33] N. Singh, R. M. Mehra and A. Kapoor. "Synthesis and Characterization of ZnO Nanoparticles", *J. Nano- Electron. Phys.* Vol.3, no. 1, pp.132-139, 2011.

[34] A. Djelloul, K. Bouzid and F. Guerrab. "Role of Substrate Temperature on the Structural and Morphological Properties of ZnO Thin Films Deposited by Ultrasonic Spray Pyrolysis". *Turk J Phys 32*, pp.49-58, 2008.

[35] N. Shakti, A. Prakash, T. Mandal, M. Katiyar. "Processing temperature dependent morphological and optical properties of ZnO nanorods", *Materials Science in Semiconductor Processing 20*, pp.55–60, 2014.

[36] S. A. Ahmed. "Structure and magnetism of manganese-doped ZnO powder samples", *Cryst. Res. Technol*. Vol.44, No. 9, pp.971-977, 2009. DOI 10.1002/crat.200900289

[37] A. Askarinejad, M. A. Alavi and A. Morsali. "Sonochemically Assisted Synthesis of ZnO Nanoparticles: A Novel Direct Method", *Iran. J. Chem. Chem. Eng.* Vol. 30, No. 3, pp.75-80, 2011.

[38] K. Zak, W. H. Abd, Majid, M. E. Abrishami, and R. Yousefi. "X-ray analysis of ZnO nanoparticles by Williamson-Hall and size-strain plot methods", *Solid State Sciences,* Vol.13, pp.251-256, 2011.

[39] M. Acosta-Humánez, L. Montes-Vides and O. Almanza-Montero. "Sol-gel synthesis of zinc oxide nanoparticle at three different temperatures and its characterization via XRD, IR and EPR", DYNA, Vol.83, no.195, pp. 224-228, 2016.

[40] M. Gupta, V. Sharma, J. Shrivastava, A. Solanki, A. P. Singh, V. R. Satsangi, S. Dass and R. Shrivastav. "Preparation and characterization of nanostructured ZnO thin films for photoelectrochemical splitting of water", *Bull. Mater. Sci.,* Vol.32, no.1, pp.23–30, 2009.

[41] A. Faisal, R. Ismail, W. Khalef, and E. Salim, A. Faisal, R. Ismail, W. Khalef, and E. Salim, *Opt. Quantum Electron.*, Vol. 52, p 1, 2020.

[42] A. G. Kaningini, S. Azizi, N. Sintwa, K. Mokalane, K. C. Mohale, F. N. Mudau, and M. Maaza, "Effect of Optimized Precursor Concentration, Temperature, and Doping on Optical Properties of ZnO Nanoparticles Synthesized via a Green Route Using Bush Tea (*Athrixia phylicoides* DC.) Leaf Extracts", *ACS Omega*, 7, pp. 31658−31666, 2022. http://pubs.acs.org/journal/acsodf Article

[43] K. W. Aga, M. T. Efa and T. T. Beyene, "Effects of Sulfur Doping and Temperature on the Energy Bandgap of ZnO Nanoparticles and Their Antibacterial Activities", *ACS Omega*, 7, pp.10796−10803, 2022. http://pubs.acs.org/journal/acsodf

[44] S. A. Kaur, G. S. Randhawa and R. Singh, "Synthesis and structural analysis of cobalt doped zinc nanoparticles", *IOSR Journal of Applied Physics (IOSR-JAP),* Volume 9, Issue 5 Ver. III, PP 18-24, Sep. - Oct. 2017. DOI: 10.9790/4861-0905031824

[45] K. Zak, W. H. Abd, Majid, M. E. Abrishami, and R. Yousefi. "X-ray analysis of ZnO nanoparticles by Williamson-Hall and size-strain plot methods", *Solid State Sciences,* Vol.13, pp.251-256, 2011.

[46] S. A. Kaur, G. S. Randhawa and R. Singh, "Synthesis and structural analysis of cobalt doped zinc nanoparticles", *IOSR Journal of Applied Physics (IOSR-JAP),* Volume 9, Issue 5 Ver. III, PP 18-24, Sep. - Oct. 2017. DOI: 10.9790/4861-0905031824

[47] E. A. Ara´ujo J´unior, F. X. Nobre, G. D. S. Sousa, L. S. Cavalcante, M. R. D. M. C. Santos, F. L. Souza and J. M. E. D. Matos, "Synthesis, growth mechanism, optical properties and catalytic activity of ZnO microcrystals obtained via hydrothermal processing", *RSC Adv.*, Vol.7, 2017. DOI: 10.1039/c7ra03277c